Designing Surface Exposed Sites on *Bacillus subtilis* Lipase A for Spin-Labeling and Hydration Studies

Afnan M. Jaufer,[a,b] Adam Bouhadana,[a] Amir Kharrazizadeh[a] Mingwei Zhou[a] Coray M.Colina, * [a,b,c] and Gail E. Fanucci*[a]

[a] *Department of Chemistry, University of Florida PO BOX 117200, Gainesville Fl. 32611.*
[b] *George and Josephine Butler Polymer Research Laboratory, University of Florida, Gainesville, FL 32611, United States.*
[c] *Department of Materials Science and Engineering, University of Florida PO BOX 117200, Gainesville Fl. 32611. United States.*

Electronic Supplementary Information (ESI) available: [details of any supplementary information available should be included here]. See DOI: 10.1039/x0xx00000x

Abstract: Spin-labeling with electron paramagnetic resonance spectroscopy (EPR) is a facile method for interrogating macromolecular flexibility, conformational changes, accessibility, and hydration. Within we present a computationally based approach for the rational selection of reporter sites in *Bacillus subtilis* lipase A (BSLA) for substitution to cysteine residues with subsequent modification with a spin-label that are expected to not significantly perturb the wild-type structure, dynamics, or enzymatic function. Experimental circular dichroism spectroscopy, Michaelis-Menten kinetic parameters and EPR spectroscopy data validate the success of this approach to computationally select reporter sites for future magnetic resonance investigations of hydration and hydration changes induced by polymer conjugation, tethering, immobilization, or amino acid substitution in BSLA. Analysis of molecular dynamic simulations of the impact of substitutions on the secondary structure agree well with experimental findings. We propose that this computationally guided approach for choosing spin-labeled EPR reporter sites, which evaluates relative surface accessibility coupled with hydrogen bonding occupancy of amino acids to the catalytic pocket via atomistic simulations, should be readily transferable to other macromolecular systems of interest including selecting sites for paramagnetic relaxation enhancement NMR studies, other spin-labeling EPR studies or any method requiring a tagging method where it is desirable to not alter enzyme stability or activity.

1. Introduction

Lipases are ubiquitous enzymes found in most organisms from the microbial, plant and animal kingdoms [1,2]. The lipase enzymes consist of a large family showing the same overall alpha-beta hydrolase structural tertiary fold[3]. In nature, they play a key role in fat metabolism and digestion by catalyzing the hydrolysis of lipids [4]. Lipases find usage as biocatalysts for ester hydrolysis, esterification and transesterification reactions involving water-insoluble esters [5]. This makes them useful in industrial and biomedical settings [6]. A large number of studies have been done on the structure-function relationship of lipases [7]. Most of these, however, have been on lipases whose enzyme activity primarily depends on interfacial activation [8]. For instance, previous studies done on pancreatic lipase shows that it exhibits little activity when the water-soluble short chain triglyceride triacetin is in the monomeric state [9]. However, after the substrate concentration exceeds the solubility limit, the hydrolytic reaction increases dramatically, with the same substrate present, in micelles or as emulsion drops. The activity is independent of the molar concentration but controlled by the concentration of substrates at interfaces. This “interfacial activation” phenomenon generally ascribes to the presence of an amphipathic mobile subdomain lid or flap located over the active site, which undergoes conformational changes in contact with the micellar substrates [8]. Hence the lid domain tends to have two conformations that govern

the activity of the lipase – the open conformation and the closed conformation – leading to active and inactive forms for the enzyme, respectively [10]. The lid is stabilized in the open state upon interaction with a hydrophobic surface, thus allowing access to the active site [11-14].

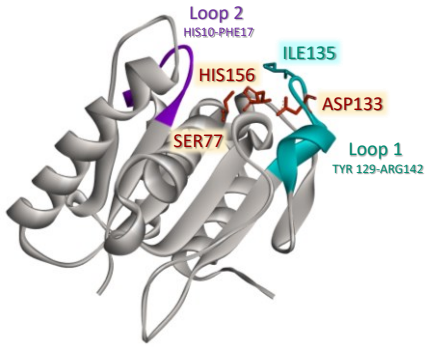

Figure 1 Ribbon diagram of *Bacillus subtilis* lipase A (PDB code: 1ISP) showing the surface exposure of catalytic triad (residues highlighted in dark orange stick format) with mobile Loop 1 (TYR 129-ARG142) annotated in cyan showing residue ILE135 that can "cap" the active site area and act as a loop to cover the active site in a lid-like manner [15], with mobile Loop 2 (HIS10-PHE17) rendered in violet.

In contrast, *Bacillus subtilis* lipase A (BSLA) does not have an extended loop or alpha helix lid structure; thus, leaving the catalytic triad relatively surface exposed (Figure 1) with no dependence on interfacial activation [16]. This difference in catalytic activation from its peers allows unique advantages for the usage of BSLA as a biocatalyst. Multiple studies of BSLA have been carried out with aims of increasing thermostability [17,18], water solubility [19], solubility in organic solvents [20,21], stability in harsh solvents [22,23], and activity as a solvent-free liquid protein (also known as biofluids or protein-liquids) [24,25]. Much of this work involves strategies that focus on modification of the protein in some manner, such as site-directed mutagenesis, bioconjugation, and immobilization [26-32]. More fundamental work has also been carried out to understand structure/function relationships of BSLA. Works by Khan and coworkers [7] have studied the lack of the lid domain in Lipases from a functional perspective, while other studies have used BSLA as a model for a minimal alpha beta hydrolase fold [3]. More recently coarse-grained molecular dynamics simulation, using ELNEDYN combined with the MARTINI force field, revealed insight into experimental observations of enhanced BSLA activity at the oil-water interface in the presence of non-covalent detergents based upon Janus behavior of the enzyme, thus suggesting that this reorientation at the interface can be a form of interfacial activation [33]. Further molecular dynamic simulations of BSLA in a substrate bound and unbound form provide evidence from principle component analysis that Loop-1 (Tyr 129-Arg142) and Loop-2 (His10-Phe17) move in the substrate-free state; giving rise to an effective lid-opening and lid-closing [15]. The authors of this work propose Loop-1, which is also seen to open up at an oil-water interface, should be considered as a lid in BSLA. Collectively, all these studies have pushed the utility of BSLA and our understanding of its substrate specificity, structural stability and overall solubility [34].

Although experimental wet-lab studies and existing simulation work have significantly contributed to the exploration of this space, it is notable that BSLA has been the focus of molecular modelling and simulation work as well. For instance, work by Zhang and Ding [35] investigated the hydrogen bonding of BSLA and its thermostable variant. Other works have characterized the surface charge effect of solubility in ionic solvents [36,37] and organic solvents [20,21,38]. Much of these *in silico* works focused on enabling an inherent utility of lipase, effectively modifying the wild-type structure in some manner to achieve an advantageous effect. The desired effect involved an

increased stability to temperature, solvent, ionic strength, or any other combination of harsh external factors to enable industrial biocatalysis.

Interestingly however, the fundamental characterization of the hydration of BSLA is known only via attempts to enhance solubility within organic solvents [20,21]. Our research seeks to fill the existing gap in knowledge to understand the surface hydration of BLSA through a spectroscopic and atomistic simulation perspective. Advances in magnetic resonance spectroscopy has enabled the use of nitroxide spin-labels coupled with electron paramagnetic resonance (EPR) spectroscopy to be used for probing a vast array of structural and dynamic properties in proteins and other biological macromolecules [39-55]. Through low-field (9.5 GHz/14.6 MHz) Overhauser dynamic nuclear polarization (ODNP) nuclear magnetic resonance (NMR) of a spin-labeled macromolecule, the water molecule hydration diffusivity within a 5-10 Å shell of the spin-label attachment site can be determined [56,57]. This allows a for a localized interrogation of the movement of water molecules in a site-selected region. Site directed spin-labelling (SDSL) is a field that is highly explored, and it has even been utilized to study lid mobility in pancreatic lipase [13]. Nevertheless, ODNP has not previously been utilized to study the hydration of BSLA. Therefore, the establishment of suitable labelling sites and their effects on the structure and function of BSLA are described within. Our approach utilized atomistic molecular dynamics simulations and analyses to help guide the rational design of a series of spin-labeled reporter sites on the surface of BSLA for usage in EPR and future ODNP investigations of BSLA in unmodified and modified forms (*e.g.,* thermostable, bioconjugates, stabile and active in organic solvents). To this end, we generated a work-flow model that relies on atomistic molecular dynamics (MD) simulations to help evaluate the perturbation that a given chemical modification has on wild type BLSA conformation and dynamics. The substituted cysteine residue by S-(1-oxyl-2,2,5,5-tetramethyl-2,5 dihydro-1H-pyrrol-3-yl)methyl methanesulfonothioate, (MTSL) could potentially impact enzymatic function, solubility and stability.

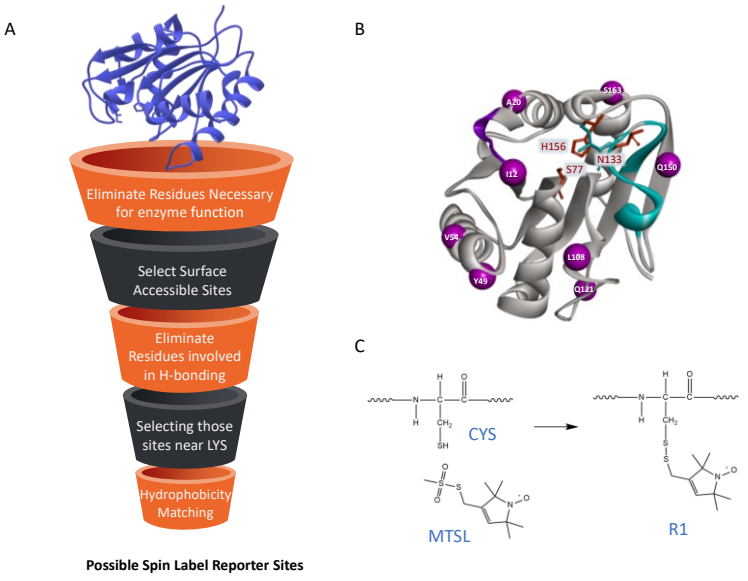

Figure 2. (A) Schematic outlining a rational approach for designing locations of CYS substitutions according to a set of desired metrics, (B) the location of the 8 sites chosen for this investigation rendered as spheres for the C_α carbons (PDB ID 1ISP) and (C) scheme for the chemical labeling of a CYS side chain with MTSL to generate the R1 side chain.

Often, the first steps in a spin-labeling strategy are to choose appropriate reporter sites that provide information on local dynamics, structural changes, and environmental conditions without perturbing the native structure, dynamics, stability or function of the biological macromolecule [45,50,58]. Matlab based Multiscale Modeling of Macromolecules (MMM) is an open-source tool box that readily allows for accessing spin-label rotomer conformations appended to biomolecules, and as such offers a starting platform to assess surface accessible sites and possible distance contraints for EPR studies [59]. Additional computational resources, such as chiLife are being developed to aid in these judicious choices of selecting reporter sites for probing structure and conformational changes via distance measurements with spin-labels [60]. Additionally, a recent review summarizes how several spin-lableing studies have combined computational approaches to aid in the analysis of the resultant EPR data [61]. Herein, we extend combined experimental and computational approaches that helped guide the judicious choice of surface CYS amino acid substitutions in BSLA for spin-labeling via MTSL that do not perturb the structure, stability or function of BSLA. A series of eight spin-labeled BSLA constructs were generated, and the impact of the CYS and spin-labeled modification is characterized both experimentally and computationally. Figure 2 graphically summarizes this approach, showing locations of the chosen reporter sites for BSLA studied here, as well as the R1 spin-labeling scheme.

2. Materials and Methods

2.1 Atomistic molecular simulations

Starting coordinates for all simulations were obtained from the 1.3 Å resolution crystal structure of BLSA (UNIPROT Accession Code P37957) PDBID:1ISP [16]. The deposited structural coordinates lack one amino acid residue at each terminus ALA1 and ASP181, which were added. All CYS variants were created using the UCSF Chimera [62] software. Side chain conformations that minimized overlaps of VDW radii between atoms were chosen. For simulations of cysteine variants, further modified with the spin label (MTSL) attachment (designated R1 as a new side chain) was done using CHARMM-GUI [63], with parameters obtained from the work of Islam and Roux [64,65]. The titratable residues of the protein were adjusted to the pH of 7.0 and the water model used was cTIP3P, forming a box with a buffer of 16 Å. Non bonded cut-off was set to 12 Å. 4 Cl^- ions were added to neutralize the charge and 63 Na^+ and 63 Cl^- ions were added to create a similar environment (300 mM NaCl concentration) to the system being studied experimentally.

The CHARMM36m [66] forcefield was selected for the protein and simulation were performed with the AMBER 20 [67] molecular dynamics engine on GPU on HiperGator 3.0 at University of Florida. WT BSLA and BSLA-R1 variants were subjected to gradient energy minimizations over 10,000 steps while holding the protein with harmonic restraints. The systems were further minimized for an additional 10,000 steps without restraint. Next, the variants were heated to 300 K in 20 ps intervals and 50 K increments using a NVT ensemble followed by 1000 ps of additional simulation. Subsequently, the NPT ensemble was applied to each system at 1 bar. Particle Mesh Ewald summation was used for long-range electrostatic interactions. Bond lengths involving hydrogen atoms were constrained using a 2 fs time step with the SHAKE algorithm. A total of 2 μs simulation were performed for each BSLA variant. Control analyses of all the simulation data were performed by monitoring RMSD (Figure S14), radius of gyration (Figure S15)

and density against time (Figure S16). In addition, Ramachandran plots for the backbone dihedral angles were analyzed as well (Figures S17 to S25)

2.2 Using H-Bonding Analysis and DSSP to Analyze Structural Features.

The hydrogen bonding interactions within the system were calculated based on a geometric criterion. The hydrogen bonding criteria used in this analysis were as follows: a hydrogen bond was considered to exist if the distance between the hydrogen-bond donor and acceptor atoms was below 3.0 Å, and the angle formed by the donor, hydrogen, and acceptor atoms was equal to or greater than 135°[62,67]. The 2 μs simulation was monitored using this method, and hydrogen bonding occupancies were calculated. All hydrogen bonds that had an occupancy equal to or greater than 30% of the total simulation were considered for the initial filter, similar to the work by Ramanathan *et al.* [68].

For investigating the secondary structures of the atomistic simulations, we used the DSSP (Define Secondary Structure of Proteins) algorithm. The DSSP is a standard method for assigning secondary structure to the amino acids of a protein, given the atomic-resolution coordinates of the protein. DSSP functions by identifying the intra-backbone hydrogen bonds of the protein using the geometrical definition outlined above. It then uses a series of criteria as mentioned in Kabsch *et al.* [69] to categorize each amino acid in the protein sequence into one of eight different categories- (1) alpha, (2) 3-10, or (3) pi -helix, (4) parallel or (5) anti-parallel beta sheets, (6) turns, (7) bends, and finally "(8) none" which is the class where amino acids that don't fit into any other secondary structure motif are classified.

2.3 Experimental BSLA Overexpression, purification, and labeling

Sites I12C, A20C, Y49C, V54C, L108C, Q121C, Q150C, and S163C were ultimately chosen for reporter sites for spin-labeling with MTSL. Mutants encoding for the desired CYS substitutions were generated by Qiagen site-directed mutagenesis kit of the template WT BLSA gene cloned into a pET21b between the cut sites *Nde*I and *Sac*I. The sequence inserted between these cut sites contained multiple stop codons to terminate translation and the expression of the C-Terminal Histag contained within the pET21b plasmid, which we obtained WT BSLA plasmid from Dr. Joel Kaar, University of Colorado Boulder. Mutagenic primers were designed and ordered from IDT (Coralville, IA) with reactions carried out according to manufacturer's suggested protocol; mutations were verified by DNA Sanger sequencing (Azenta-Genewiz, South Plainfield, NJ). Plasmids encoding wild-type BLSA and cysteine substituted variants were each transformed into BL21(DE3)pLysS competent cells which were then grown in 1 L LB media at 37 °C at 250 rpm until optical density at 600 nm (OD600) was between 0.6 and 0.8. Subsequently the expression of BLSA was induced by 1mM IPTG (isopropylthio-β-galactoside) for 24 hours. Isolation and purification of non-histagged BSLA ensued from inclusion bodies based upon purification schemes previously reported by others [19,22,26]. Cells were harvested at 6000 RCF for 15 minutes at 4 °C and the obtained pelleted cells were resuspended in 10 mM Na_2HPO_4, 50 mM NaCl buffer at pH 8.0, along with 100 μL of protease inhibitor cocktail mix G6521 (Promega Corporation, Madison, WI). Cells were lysed via tip sonication (Fischer Scientific Sonic Dismembrator-Model 100) in 5 second intervals for 2 minutes, tubes inverted and repeated 3 times, with the cell solution kept on ice for the 6 minute time period. After sonication, the solution was centrifuged at 17000 RCF for 10 minutes at 25 °C. The insoluble portion, which included cell debris and the inclusion bodies containing BLSA, was retained and dissolved in 5 mL of 6M Guanidine hydrochloride using a mortar and pestle, if necessary.

The resulting solution of unfolded BLSA was refolded by slow dropwise addition to a solution of 10 mM Na_2HPO_4 buffer at pH= 7.0 (volume 20x dilution) and then centrifuged at 17000 RCF at 25 °C. The supernatant from this step was retained and filtered through a 0.2 microfilter and applied to a 5-mL cation exchange sepharose column (Hitrap SP Sepharose, Cytivia, Pittsburgh, PA) via an AKTA Prime FPLC system, which was equilibrated with buffer (10 mM monobasic sodium phosphate at pH 5.5), followed by five column volumes of washing with the equilibration buffer and eluted using a similar buffer of higher ionic strength (10 mM monobasic sodium phosphate, 500 mM NaCl at pH 7.0). For CYS variants, DTT was added to each fraction that contained protein to ensure the reduction of any disulfide bonds formed. The final concentration of DDT was 1 mM (~ 5x protein concentration). The purity of the fractions was assessed via SDS-PAGE. Suitably pure fractions that showed a single band in the 20 kDa region were pooled and concentrated via an Amicon 10 kDa cutoff centrifugal filter unit prior to buffer exchange to 10 mM monobasic sodium phosphate pH 7.0, via a Hi-Prep 26/10 desalting column. This step also ensured any DTT in the solution was removed. Immediately after this, spin labeling of BLSA cysteine constructs with MTSL (S-(1-oxyl-2,2,5,5-tetramethyl-2,5 dihydro-1H-pyrrol-3-yl)-methyl methanesulfonothioate) was performed. MTSL (~ 0.5 mg) was dissolved in 50 µL of ethanol and an appropriate volume was added to give ~ ten-fold molar excess to the BLSA solution concentration (note: sample has five-fold DTT) and reaction was allowed to proceed overnight at 4 °C. Excess spin label was removed using the Hi-Prep 26/10 desalting column, doing a final buffer exchange into 2.5 mM monobasic sodium phosphate, 21.5 mM sodium chloride, pH 7.0. This choice of buffer allowed samples to be concentrated to a level targeted for future spectroscopic and hydration studies [22]. The sample was once again concentrated via the Amicon 10 kDa cutoff centrifugal filter to ~ 200 µM. Enzyme concentration was determined using the bicinchoninic acid assay and corroborated by measuring optical density at 280 nm at which the theoretical molar extinction coefficient of the enzyme is 24,410 $M^{-1}cm^{-1}$ [26]. Spin-labeling was confirmed via Mass Spectrometry analysis (Table S8)

2.4 EPR Data Collection

A Bruker E500 spectrometer with a dielectric resonator was used to collect CW X-band EPR spectra. For all experiments the temperature was kept at a constant 27.0 ± 0.3 °C using air passed through a copper coil submersed into a water bath, while monitored with a temperature probe and thermometer from OMEGA Engineering Inc (Norwalk, CT) as described in detail earlier.[70] Samples were loaded via capillary action in cleaned and dried (0.50 inner-diameter. x 0.84 outer-diameter) suprasil capillary tubes and sealed with Cha-seal from Fisher Scientific Inc (Hampton, NH) tube sealing compound. All spectra are reported as an average of 20 scans, collected as 100 G sweep width, 0.6 G modulation amplitude, 25 ms conversion time, 100 kHz modulation amplitude, and 2 mW incident microwave power. Spectra were normalized using LabVIEW-based software (obtained from Christian Altenbach/Wayne Hubbell) allowing for baseline correction and double integral area normalization.

2.5 EPR Line Shape Fitting

EPR spectra were fit using *chili* and *esfit* functions of EasySpin,[71] with the following values for the **A** and **g**-tensors: A_{xx}= 6 G, A_{yy}=6 G, A_{zz}= 37 G, g_{xx}=2.0089, g_{yy}= 2.0021, g_{zz}= 2.0058. [72-75] Other parameters used in the EPR line shape fitting include linewidth (which can be reflective of spin-spin interactions), correlation time of motion (τ_c), and the ordering potential C_{20}, which was used to calculate the motional order parameter *S*.[72-75] Fitting results of all R1-BSLA EPR spectra are reported as single component fits in Table S-9 and shown in Figure S12.

2.6 CD Data Collection and Analysis

All CD spectra were obtained over the wavelengths of 190 to 260 nm on a Chriascan V100 CD spectrometer (Applied Photophysics Inc, Charlotte NC) with a quartz cuvette to minimize absorption any extra absorption in the lower wavelengths. The buffer for each sample was 2.5 mM monobasic sodium phosphate, 21.5 mM sodium chloride at pH 7.0. Three separate protein samples from an individual expression/purification/labeling batch were prepared to provide triplicate data. The CD spectra were obtained at 25 °C, and the thermal melts were obtained over a range of 20-90 °C by monitoring the value of molar ellipticity at 222 nm (θ_{222}) as a function of temperature. Values of θ_{222} were converted to fraction of unfolded protein, which was then analysed as a function of temperature through sigmoidal shaped fits to obtain values for T_m, which is the temperature at which the fraction of folded state available is at 0.5. The derivative of the sigmoidal fit generates a Gaussian shaped curve, where the full width at half maximum (FWHM) provides an assessment of the degree of cooperativity of the transition.

2.7 BSLA Enzymatic Activity Assays

Enzyme kinetics experiments were carried out for WT and all R1 spin-labelled variants. The experiment was conducted using a Varian Cary (Agilent, Santa Clara CA) 50 UV/Visible spectrophotometer, equipped with a Peltier-based temperature control system to maintain a constant temperature of 25°C. The substrate used was p-nitrophenyl butyrate (pNPB), which was dissolved in acetonitrile at a concentration of 50 mM [19]. The final buffer of the solution composition was 2.5 mM monobasic sodium phosphate and 21.5 mM sodium chloride, adjusted to a pH of 7.0. The final enzyme concentration for each system was 10 µM (added from a stock of 200 µM concertation), with the varied final substrate concentrations of 1.0, 2.0, 4.0, 5.0 and 10.0 mM. Each experiment with a specific substrate concentration was conducted in triplicate. Hence, each experiment consisted of a 1 mL quartz cuvette with a pathlength of 0.1 cm was loaded with the reaction mixture containing the pNPB substrate, BSLA buffer, and finally, the enzyme. The spectrophotometer was set to measure the absorbance of the reaction mixture at the wavelength of 420 nm for a period of 10 minutes. The collected absorbance data were subsequently analyzed to provide the initial reaction rates. To account for any self-degradation of the substrate, a control measurement was also performed alongside each enzyme catalyzed hydrolysis experiment. The control samples included all reagents except for the enzyme, and rates of self-degradation of substrate were subtracted from the enzyme catalyzed rates. From the corrected initial velocity values, the Michaelis-Menten kinetic parameters were then determined from the corresponding Lineweaver-Burke plots.

3. Results and Discussion

3.1 Criteria and Methods for Choosing Sites for Cysteine Modification in BSLA

Nitroxide spin-labels are oftentimes incorporated into biomacromolecules through chemical modification of a unique cysteine residue [47,49]. Given WT BSLA has zero naturally occurring CYS, it offers a natural template for our studies. Our overall goal is to generate a series of SL reporter sites around the surface of BSLA such that ODNP and EPR can be utilized to interrogate how polymer conjugation [22,26,37] or amino acid engineering [20,21,76] impact surface mobility and hydration. Additionally, various studies show that the thermostability of BSLA is easily altered by amino acid substitutions, hence, it is not trivial to predict which surface locations on BSLA will retain stability. Furthermore, we desire sites of spin-label incorporation that provide a strong

"signal" of interaction with the biopolymers, a probe of surface hydration near the site of bioconjugation, and where local dynamics are similar amongst sites in the absence of bioconjugation, where in the native state these sites can be exquisitely sensitive to changes in molecular crowding, solution polarity and hydration. For the present studies, this means spin-labelled sites that result in high side-chain nitroxide mobility; thus, giving rise to EPR line shapes at X-band frequency that are reflective of the fast-limit regime (τ_c ~ 0.5 to 1-2 ns),[43,47,48,77,78]. In this way, reporter sites on BSLA will be expected to probe the local hydration environment of different areas of the protein in different forms (e.g., polymer conjugates versus native versus modified constructs). For this purpose, we chose the following criteria for filtering potential sites for labelling:

A. Reporter site should not affect known function. Sites identified by others in the literature as essential for function were discarded [16,79,80].

B. Must be solvent accessible. The spin label cannot be crowded by other elements of the protein. Hence, this positive filter selected those residues identified with > 50% relative solvent accessibility (RSA). Although this value can be determined using an existing PBD structure and analysis of spin-label rotamers via MMM [59], within we utilized the average from obtained from atomistic simulations to allow for molecular motions and to minimize potential crystallographic artifacts from crystal-crystal packing.

C. Minimal perturbation to thermal stability and catalytic activity. The hypothesis here is that H-bonding is important for catalytic activity and thermal stability and as such the spin-label should not replace an amino acid that is involved in the H-bonding network of the protein This step removed sites with > 30% occupancy of a H-bond within the protein determined from atomistic simulations.

D. The site should be near the surface accessible LYS residues that will be the future anchoring sites for conjugation of polymer chains, as this closeness should induce alterations in mobility and hydration. In this step, we discarded surface LYS residues and the N- and C-terminal sites and positively selected for those sites remaining that were within a 5 Å shell of the LYS sites previously identified as likely location for bioconjugation [26].

These steps are graphically depicted in Figure 2 with the resultant sites chosen for modification to R1 shown in Figure 3.

Step A: Identifying Functionally Relevant Residues.

Typically, the first step in any labeling study is to discard sites known to be important for function. BSLA is a globular protein of 181 residues bearing the alpha-beta hydrolase fold [3]. The alpha-beta hydrolase fold belongs to the doubly wound alpha-beta superfold in the Structural Classification of Proteins (SCOP) classification standard. The components of the common alpha-beta hydrolase fold include a central, parallel β-sheet with eight beta strands, where only the second strand (β2) is antiparallel, along with six α helices on the sides of the central β-sheet that connect the strands β3 to β8. Prior studies of others have outlined residues that comprise the active site [16] as well as those having critical interactions with the active site shown to modulate enzymatic activity [80]. These include the catalytic pocket [81], the oxyanion hole [82], which stabilizes the substrate in the transition state, and a 9-amino acid region containing hydrophobic residues described by some as a lipid-binding segment [83]. These ten identified residues, (D40, F41, W42, D43, K44, T45, G46, S77, D133, H156) were removed (Negative Filter 1) from consideration of CYS modification.

Step B: Determining the Relative Solvent accessibility of BSLA

To provide a quantitative metric for identifying solvent accessible residues, the relative solvent accessible surface area was calculated for all residues. In this study, the per-residue solvent accessible surface area (SASA) is calculated by averaging the per-residue SASA over 2.0 μs of the molecular dynamics production. Given the solvent of consideration is water, the calculation for SASA necessitates the use of a 1.4 Å "probe radius" [84]. This means that a sphere of radius 1.4 Å is "rolled" over the surface of the molecule, and the surface area that is traced by such a sphere is taken to be the absolute SASA. Based on SASA values, amino acid residues of a protein can be classified as buried or exposed.

There are various methods of quantifying SASA, from relative solvent accessibility to absolute surface areas. Here, we chose to utilize the relative surface area (RSA) as the selection parameter. To calculate the *relative* surface area (RSA), a normalization factor is used for each amino acid. By convention, these normalization values are derived by evaluating the maximum surface area around a residue of interest X when placed between two glycines, to form a Gly-X-Gly tripeptide [85]. The reason for doing this is to be able to use a residue specific normalization method that encapsulates a suitable upper bound absolute SASA. The normalization values for each amino acid calculated this way is reported by Tien *et al.*[85] (given in Table S1). Upon calculating the absolute per residue SASA for BLSA, each value was divided by its respective normalization value as to give results plotted in Figure 3. Those residues with RSA < 0.5 were discarded as potential sites for spin-labeling, leaving 38 possible surface exposed sites for consideration. It is worth noting that although the N- and C- termini of the graph show very high RSA values, consistent with being located at the N- and C- termini of the protein, and also because the normalization values for each residue are obtained by considering absolute SASA values from the gly-X-gly tri-peptide model, these were discarded as potential spin-label reporter sites in a later filter. As expected from the crystal structures of BSLA, the highly buried residues often correspond to the beta-sheet secondary structures, which are shown in yellow on the x-axis in Figure 3.

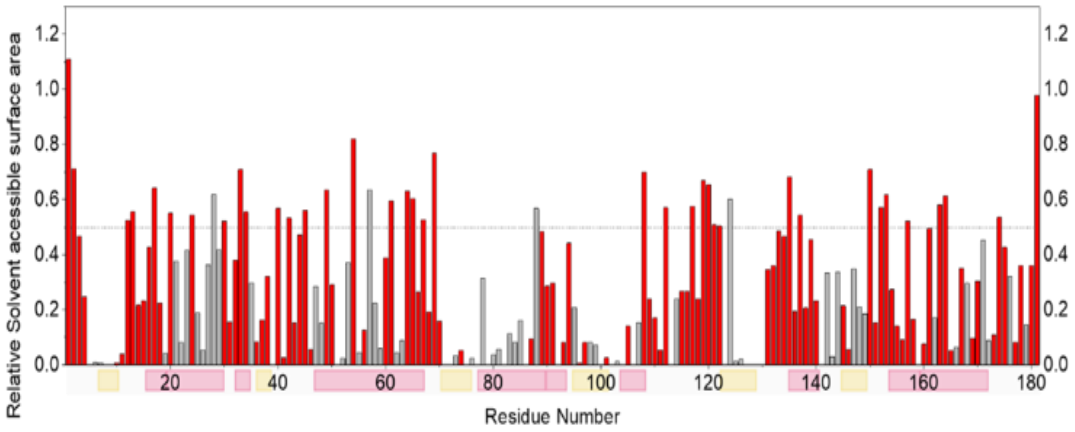

Figure 3. Bar graph of RSA for each residue of BSLA. The x-axis is color coded based on the type of secondary structures the residues are part of. Pink and yellow being representative of helices and beta sheets respectively. Residues with RSA < 0.5 (dotted line) were discarded as possible reporter sites. Bars rendered in grey represent residues identified via MD simulations as those involved in > 30% fractional occupancy of H-bonds with the catalytic center of the enzyme or being critical in enzyme functionality as reported by others in the literature.

Step C: Hydrogen Bonding Analysis

The *cpptraj* module [86] from the AMBER software package was utilized to analyze the trajectory files generated from the atomistic simulations. Specifically, the module was employed to calculate and identify hydrogen bonding interactions within the system based on a predefined geometric criterion. The hydrogen bonding criteria used in this analysis were as follows: a hydrogen bond was considered to exist if the distance between the hydrogen-bond donor and acceptor atoms was below 3.0 Å, and the angle formed by the donor, hydrogen, and acceptor atoms was equal to or greater than 135° [62,67]. The 2 μs simulation was monitored using this method, and hydrogen bonding occupancies were calculated. As defined in the work by Ramanathan *et al.* [68], hydrogen bonds that had an occupancy equal to or greater than 30% of the total simulation were evaluated as possible imporant interactions for enzymatic activity, and thus discarded within this filtering step. The list of H-bonding residues hence generated were used as a negative filter (*i.e.*- any residue on the list of H-bonding residues will eliminated from our list of potential spin-labelling sites). Filter C, brings our list of potential labelling sites from 38 to 33, revealing that only 5 surface exposed sites (S28, R57, K88, L124, and N174), which were previously not already identified as important for enzymatic activity (note surface accessible sites D40, W42, and T45 were exluded in Step A) posses > 30% hydrogen bonding interactions within the protein to the catalystic pocket. The relative H-bonding occupancy for each discarded residue is summarized in Table S2. All H-bonds were calculated based off geometric criteria [62,67] for the entire simulation.

Step D: Identifying Sites Near Surface Exposed LYS Residues.

Surface accessible LYS residues are often used as attachment sites for protein-polymer conjugation. Chado and coworkers have used PAcMO (poly-acryloyl morpholine) polymers attached in this manner to create ionic liquid-stable BSLA constructs [26]. Hence, the proximity to any surface LYS residue was used in this case to further filter the list of potential labelling sites. Surface LYS residues at positions 61, 69, 88, 112 and 122 are hence not chosens as sites for CYS modification, leaving 29 possible locations. The N- and C-terminal sites were also removed from consideration within this step (A1, E2 and N181), bringing available sites to 26.

Because our future goals are to investigate how polymer conjugation to the surface LYS alters hydration, accessibility and local dynamics, all residues within a 5.0 Å zone of each of these polymer grafting sites were identified with the use of UCSF Chimera [62]. These data were used to create a positive filter, which could be used to identify all potential labelling sites within close proximity to potential polymer attachment sites. This criterion brings our list down from 26 to 8. The identity of the amino acids remaining were I12, G13, A20, V54, L108, N120, Q121, and Q150. Sites G13 and N120 were further discarded from this list, mostly because of their proximity to other potential labelling sites of I12 and Q121; additionally, we avoided glycine as a site for CYS substitution. To produce control reporter sites that had all the vital features except for the proximity to LYS polymer attachments sites, two residues that were filtered out during Filter D were added back to the list, Y49 and S163. These two sites were chosen as they were the furthest apart from each other. These adjustments give us the final list of labelling sites that were explored in this study: I12, A20, Y49, V54, L108, Q121, Q150, and S163 shown in Figure 3.

It is instructive to list all possible surface sites without the restrict location of being within a 5.0 Å zone of surface LYS sites. This list of 26 potential spin-labeling sites includes I12, G13, F17, A20, S24, G30, R33, D34, Y49, V54, D64, E65, G67, L109, T117, P119, N120, Q121, I135, M137, Q150, H152, G153, I157, S163, and Q164. In general, other factors to consider when choosing labeling sites would be to generally avoid susbstituting glycine and proline residues and trying to match the relative hydrophobicity of the spin-labeled CYS residue. As such, acidic sites and those that can participate in salt-bridge interactions are also typically avoided.

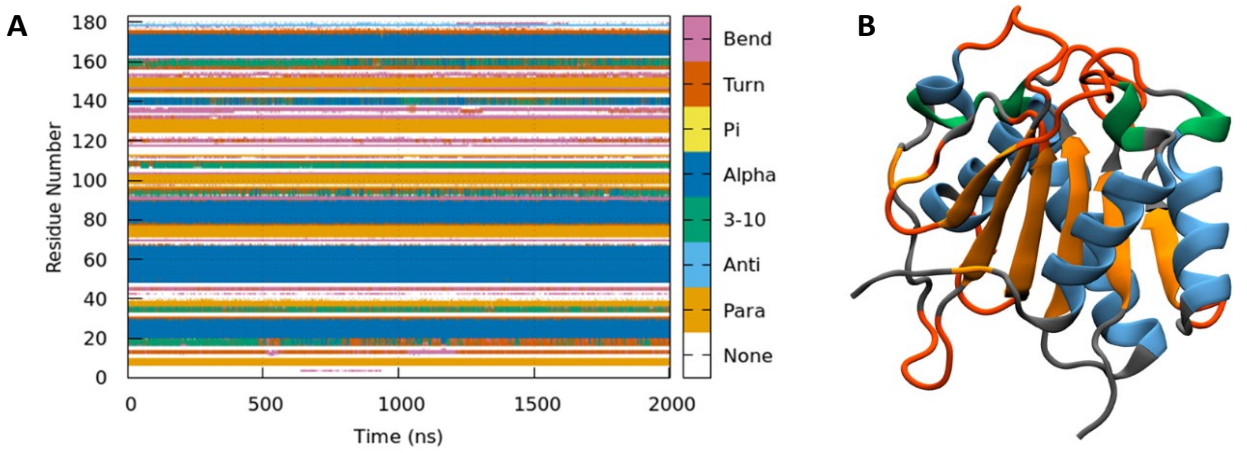

Figure 4. (A) DSSP results for WT BSLA showing secondary structure assignment for a given residue over the simulation time course and (B) resultant MD secondary structure assignments mapped onto the crystal structure ribbon diagram of BSLA (PDB ID 1ISP).

3.2 Secondary Structure Analysis of R1-BSLA Variants.

Both atomistic molecular dynamics simulations and circular dichroism (CD) spectroscopy were used to assess the impact of the R1 substitution on BLSA structure. DSSP analysis [69] of the 2 μS simulation data of wild-type and each spin-labeled BSLA construct was performed. DSSP results for WT BSLA are plotted as shown in Figure 4 where for each residue the secondary structure type is assigned a color, and the traces plot the secondary structure type over time. The general trend observed is an overall lack of changes in the secondary structure over time for WT and all R1 labeled BSLA constructs investigated.

Experimental CD spectra of BSLA variants (Figure 5) have similar overall spectral features as WT BSLA, but minor differences are observed. Further analysis of the spectra of wild type via the Bet-Stel [87] server yielded the constituent percentages shown in Fig. 5 inset. This processing was performed for all BSLA R1 variants (Table S3) and the changes of secondary structural elements compared to wild type are given in Figure 6A. Figure 6B plots an analogous analysis of the atomistic simulation data, which was analysed by the DSSP algorithm. Overall, incorporation of the R1 substitution had minor perturbations on BSLA structure, with both CD and MD analyses showing most changes to be < 10% where the highest fluctuations occur in regions containing secondary structures identified as “turns” or “others”. Importantly, these comparisons demonstrate the robustness of the MD methods for evaluating the impact of the R1 substitution on the overall protein secondary structure. The perturbations are small, and for the most part track exceedingly well with those detected via CD spectroscopy.

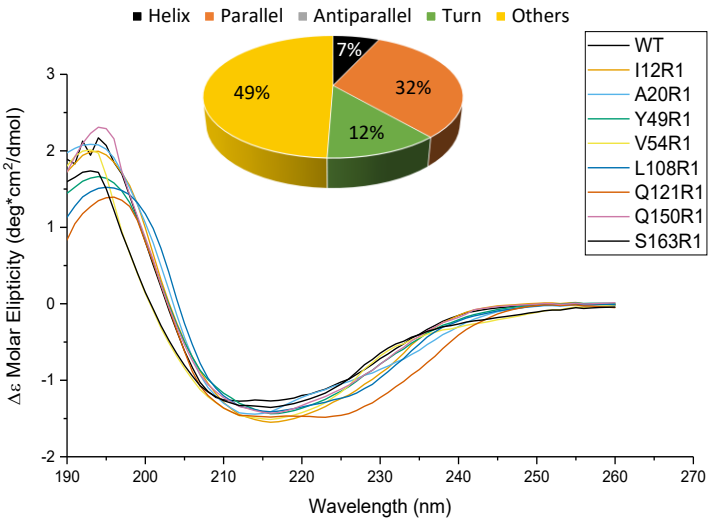

Figure 5. Overlay of experimental CD data for WT and R1 BSLA variants. Inset showing pie-chart depicting relative percentages of secondary structural elements for WT BSLA as evaluated with BeStSel [87].

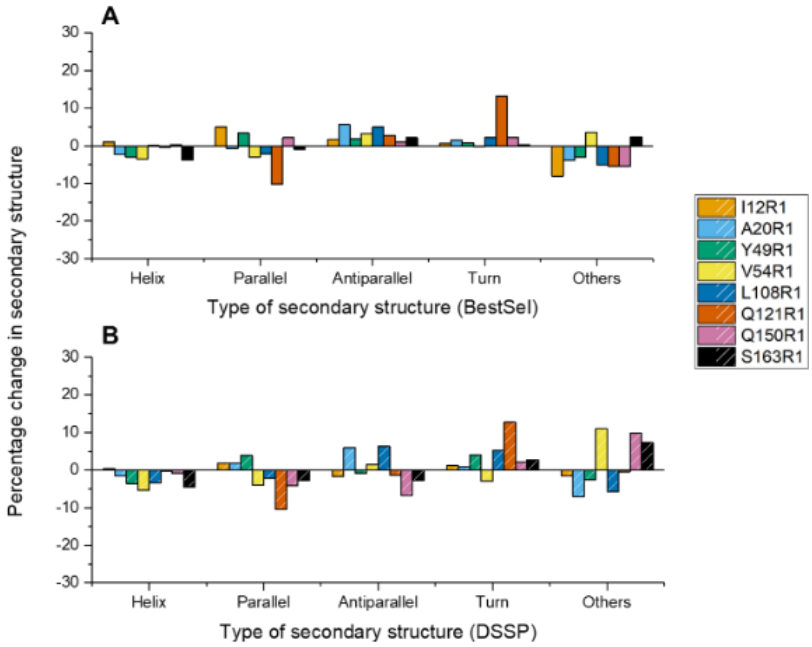

Figure 6. (A) Graph summarizing the impact of R1 substitutions on experimental CD spectra of BSLA compared to WT. Data were analyzed with BeStSel [87]. (B) Graph summarizing the impact of R1 substitutions determined from DSSP analysis of 2 µS simulation data.

The largest change in secondary structure is observed for Q121R1, which has undergone a decrease in parallel beta sheet character and an increase in “turn” typed secondary structure. These observations are recapitulated in both the experimental and computational studies (Figure 6). Previous studies have shown that disruptions in the parallel sheets of the BSLA can affect its overall fold, and hence destabilize the protein [88]. Hence, we measured the thermal stability of all constructs via CD spectroscopy. Results are shown in Figure 7. where the Q121R1 variant has the lowest T_m at 54 ± 2 °C; albeit only a 5% difference from WT with T_m = 56.7 ± 0.7 °C

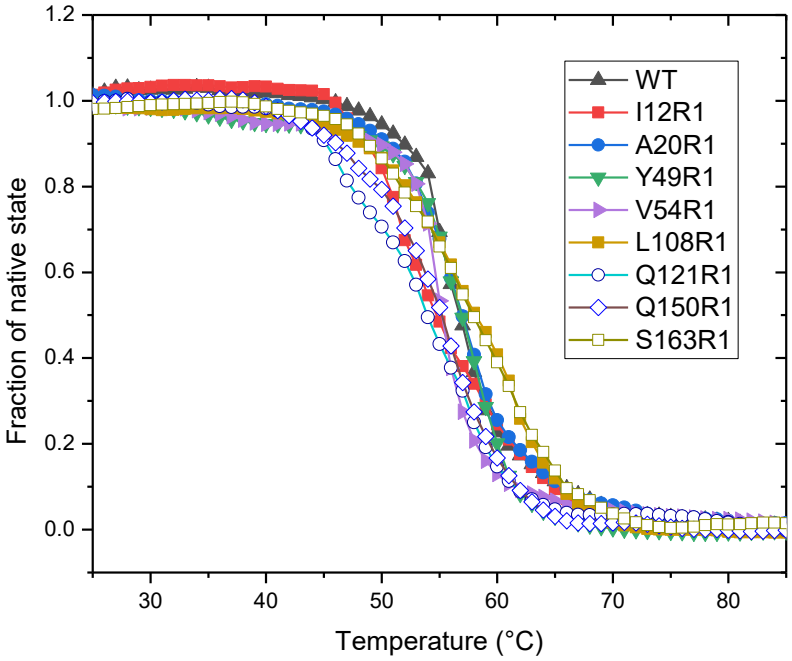

Figure 7. Thermal stability of BSLA R1 variants determined from CD spectroscopy melting curves showing fraction of the native state as a function of temperature. T_m values determined from the midpoints of sigmoidal fits to the melting curves (Given in Figures S2-210) are summarized inTable 1.

Overall, most sites chosen showed less than 10% difference in secondary structure elements with less than 5% change in thermal stability, with the largest perturbations of R1 incorporation at the Q121 site. This is noteworthy, as the site of Q121 is located on a loop and is relatively mobile as shown by our RMSF calculations of the atomistic simulation data. Studies by Nestl and Hauer [88] have shown in similar alpha/beta hydrolase fold-type proteins however, that modification of loops directly connected to the main parallel sheet core/twisted-sheet core tend to affect the stability and functionality of the protein. Inspection of the 3D structure of the protein shows us that the Q121 site lies on a loop directly connected to the main beta-sheet core of the protein.

Table 1. Kinetic and thermal stability parameters of spin-labeled variants compared to WT BSLA.

Variant	K_m (mM)	k_{cat} (min-1)	k_{cat}/K_m $(x10^{-2}mM^{-1}min^{-1})$	*Relative Catalytic Efficiency*[a]	T_m (°C)
WT	0.44 ± 0.05	600 ± 140	13.5 ± 1.8	1.00 ± 0.14	56.7 ± 0.7[b]
I12R1	0.36 ± 0.04	420 ± 90	11.8 ± 1.7	0.87 ± 0.14	55 ± 1
A20R1	0.52 ± 0.02	690 ± 50	13.2 ± 1.6	0.97 ± 0.13	56.9 ± 0.9
Y49R1	0.25 ± 0.04	290 ± 50	11.8 ± 1.9	0.87 ± 0.16	56.9 ± 0.8
V54R1	0.36 ± 0.05	440 ± 40	12.4 ± 1.4	0.91 ± 0.12	55.4 ± 0.7
L108R1	0.25 ± 0.04	280 ± 10	11.3 ±1.5	0.83 ± 0.13	58 ± 2
Q121R1	0.37 ± 0.05	410 ± 80	11.0 ± 1.4	0.81 ± 0.11	54 ± 2
Q150R1	0.27 ± 0.04	350 ± 100	12.9 ± 1.8	0.94 ± 0.14	55 ± 1
S163R1	0.42 ± 0.04	630 ± 150	14.7 ± 2.3	1.08 ± 0.19	58 ± 2

[a] $k_{cat}/K_m/(k_{cat}/K_m)_{WT}$; [b] This value is consistent with that reported by Rao and co-workers for WT BSLA expressed in soluble form [19].

3.3 Enzymatic Activity of R1-BSLA Variants

The impacts of the R1 substitutions on BSLA enzymatic activity were assessed using the chromogenic substrate para-nitrophenol assay (PNPA). Michelis Menten kinetics parameters were calculated for each variant from triplicate experiments (Results shown in Tables S4-S7) with a given purification of R1 labeled protein. Table 1 summarizes results of these studies showing that all R1 constructs have comparable enzymatic activity to WT within the 95% confidence interval as validated by a *t*-test (Figure S11). Together, the experimental data demonstrate that the R1-BSLA variants are structurally and functionally comparable to WT, with spin-labeling at site Q121 showing the largest changes relative to WT. Interestingly, although I12R1 resides within the mobile loop-2, proposed to act as part of a mobile lid in BSLA [15], susbtitution at this site did not significantly alter the secondary structure or kinetic activity of BSLA.

3.4 EPR Spectra of the R1-BSLA Variants

It has been shown that the X-band EPR spectrum of the R1 spin-label on proteins is modulated by motional averaging that arises from several sources such as protein backbone motions and local side-chain fluctuations that generate specific lineshape features that track with secondary structure [47,48,74,75]. Specifically, SDSL studies on T4 lysozyme (T4L) and other proteins have utilized lineshape parameters of the inverse central linewidth, ΔH_0^{-1}, and inverse second moment $\langle H^2 \rangle^{-1}$ to cluster EPR spectra in an effective phase space that correlates with locations in loops,

surface exposed helices and beta-sheets, sites of tertiary contact and buried locations [89,90]. Because motional averaging narrows the X-band nitroxide EPR spectrum, R1 located in loops generates an EPR spectrum with higher inverse values of both line shape parameters whereas R1 located in buried sites of the macromolecules have spectra with smaller inverse values of both parameters. SDSL studies of the GCN4 leucine zipper, which is a coiled double helix that binds to DNA, provide a detailed analysis of the R1 side chain dynamics from experimental and simulations defining the inverse central linewidth, ΔH_0^{-1}, as a semiquantitative measure of mobility of the nitroxide chain [74]. In that study, a parameter called the scaled mobility, M_s, is defined to normalize the central linewidth in comparison to other spectra reported in the literature.

$$M_S = \frac{\delta_{exp}^{-1} - \delta_i^{-1}}{\delta_m^{-1} - \delta_i^{-1}} \quad (1)$$

Where δ_{exp} is the central linewidth of R1 of the current experimental data and δ_m and δ_i are corresponding values representing mobile and immobile sites observed for R1 in proteins. We note that these values are somewhat arbitrary and for usage here we used the procedure utilized by Columbus *et al.* where values of 2.1 G and 8.4 G were utilized as limiting values; respectively [74]. The values of M_s range typically from 0 to 1, with 1 indicating high mobility and 0 indicating restricted mobility. EPR spectra were also fit using *chili* and *esfit* functions of EasySpin [71] to obtain correlation times (Figure S12; Table S9). Table 2 summarizes values of ΔH_0^{-1} M_s and τ_c for each R1-labeled BSLA construct studied here. Our initial goal was to utilize computational analyses to predict site that once labeled with R1 would give "fast limit spectra, with τ_c ~ 0.5 to 1-2 ns. Results show τ_c values span 0.7 to 1.7 ns, indicating the design strategy was successful in providing labeling site with the desired EPR spectral mobility.

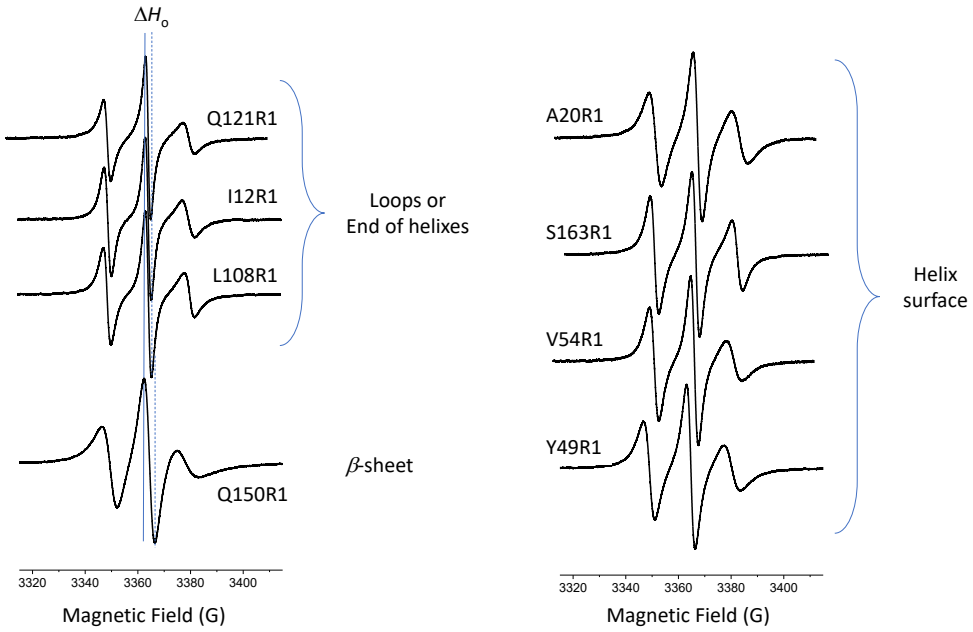

Figure 8. 100 G X-band EPR spectra for R1-BSLA plotted with normalized central line intensity and grouped according to secondary structure-type predicted by structural models. Spectra are plotted with normalized central line intensity.

The CW (X-band) EPR spectral line shapes of the 8-spin labeled R1-BSLA constructs are shown in Figure 8 and are grouped according to the secondary structure components observed in the X-ray co-ordinate structure (PDB ID 1ISP), and for which DPPS analysis of our atomistic simulation agree. This effective phase space analysis of the EPR spectra shown in Figure 8 is plotted in Figure 9; showing excellent agreement with the EPR spectral features and structural components where they reside in BSLA.

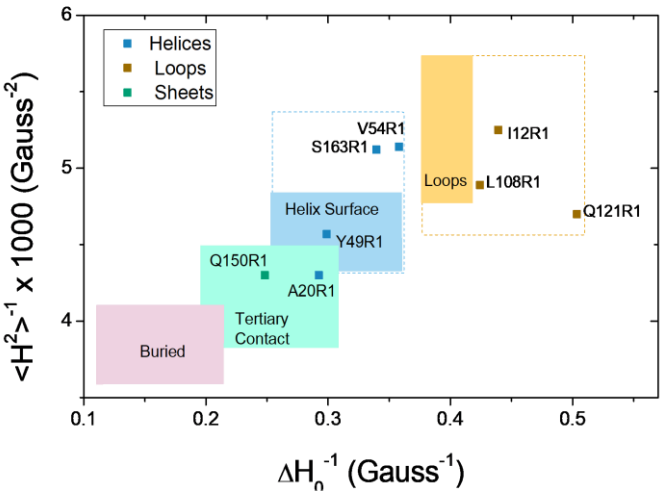

Figure 9. Plot of the inverse second moment (for 100G integral area normalized scan) versus inverse central linewidth for R1-BSLA EPR spectra compared to data reported in the literature for R1 incorporated into loops (gold), helical surfaces (blue), tertiary contact in helices and sheets (green) and buried locations (pink) [48].

Table 2. Summary of EPR line shape parameters for R1-BSLA. [a]

Variant	ΔH_{pp} (±0.05G)	M_s (±0.03) [a]	τ_c (± 0.1 ns) [b]	*Structural element*
I12R1	2.28	0.89	0.9	loop
A20R1	3.40	0.49	1.1	helix
Y49R1	3.21	0.54	1.2	helix
V54R1	2.96	0.61	1.2	helix
L108R1	2.36	0.85	0.8	loop
Q121R1	1.95	1.11	1.2	loop
Q150R1	4.17	0.34	1.8-2.2	Beta sheet
S163R1	2.86	0.65	0.8	helix

[a] M_s is calculated as described by Hubbell and co-workers.[74]
[b] Determined from fits with Easy Spin[71] using parameters reported by Hubbell and co-workers. [72-75]

Sites Q121R1, L108R1 and I12R1 are in loop regions of BSLA and have spectra with $M_s > 0.8$ and ΔH_0^{-1} and $\langle H^2 \rangle^{-1}$ that cluster in the highly mobile region of this phase space with spectra consistent to those of other proteins that are labeled within "loop regions". Inspection of the BSLA structure reveals that I12R1 is in a mobile loop, Q121R1 occurs at the end of a surface exposed beta-strand,

which has higher crystallographic b-factors than the buried beta-sheets of BSLA, and L108R1 appears at the edge of a small helical turn. All these structural sites would be expected to generate R1 spectra reflective of high mobility, as the results confirm.

The most immobile spectrum is observed for site Q150R1, which resides in the middle of the surface exposed face on the outermost beta-strand of BSLA. The backbone structure of the beta-strand is expected to provide the decreased mobility of the nitroxide seen at this site. In general, analysis of R1 mobility within beta-sheets can be problematic due to local interactions [91-93], however, the results obtained within are consistent with our expectations. The remaining four R1 sites all reside on the surface of alpha helices. A20R1 resides within the middle of a surface helix, with V54R1 and S163R1 occupying a position near to the helical ends. Although Y49R1 appears near the end of the helix, this site might come into tertiary contact with other surface residues of the nearby helix. Overall, the lineshape analysis of the X-band EPR spectra confirms the expected surface location with little to no tertiary contact.

3.5 Mobility from MD Atomistic Simulations

As discussed above, one of the motions that affects the nitroxide EPR spectral lineshape is the mobility of the protein backbone. The mobility of the backbone of WT- and R1-BSLA constructs can be evaluated via RMSF calculations (Figure 10A). Additionally, RMSF calculations of each BSLA variant compared to WT to generate ΔRMSF values (Figure 10B) reveal if and how incorporation of the R1 side chain modulated mobility compared to WT BSLA, which reveals deviations in mobility by the incorporation of the R1 substitutions, with the locations of the spin labels annotated in the graph. When analyzing these data, the C- and N- termini of each construct (and their deviations from WT) were disregarded; as termini are unstructured and hence exhibit a large conformation space that cannot be effectively sampled across simulations.

Figure 10 B shows deviations in mobility from WT for regions of residues 10-20, 110-120 and 130-140 as the ΔRMSF values in these regions exceeded a 0.88 Å cutoff, which represents the the range of the RMSD values of WT BSLA for its 2 μs simulation. Of these, DSSP analysis shows residues 10-20 are observed to switch back and forth for short periods of time between a 3-10 helix and bend conformation and 130-140 switch back and forth between a 3-10 helix and α-helical conformation (Figures 4A and S13). Hence, we attributed the small differences seen in mobility across these residues to be attributed to the arbitrary definitions used in each method to sample this type of structural transition. Sampling of such transitions is beyond the scope of the work presented here, which might require enhanced sampling methods, such as the use of adaptive steered molecular dynamics by Zhuang and coworkers.[117] The remaining region of perturbed mobility is seen for residues 105-120, and is most dramatic for constructs V54R1 and Q121R1 compared to WT. The impact of the Q121R1 substitution on mobility of its local region may not be surprising given this residue occupies the end of a beta strand where the substitution is shown via CD and DSSP analysis (Figure 6) to increase turn characteristic and remove beta structure, as shown in the increased dynamics seen in the atomistic simulations. We also see experimentally that the Q121R has the largest perturbations in enzymatic activity and thermal stability when compared to WT and the other R1-BSLA constructs (Table 1). In contrast, site V54R1 is distally located from the 105-120 region, but by hydrophobic cluster analysis via Protein Tools [94], V54 is contained within a hydrophobic cluster connected to the unstructured loop 110-122 through hydrophobic contacts to L114. V54R1 retains 90% catalytic efficiency and only shows a 2°C decrease in thermal stability. So, although this substitution appears to impact dynamics via

atomistic simulation, there is only a minor perturbation on thermostability and enzymatic function.

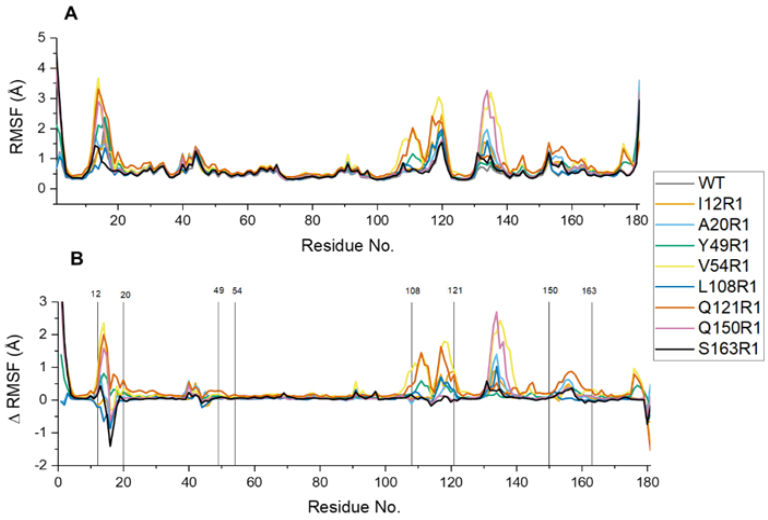

Figure 10. (**A**) RMSF plot as a function of residue number for WT and all R1-BSLA constructs. (**B**) Plot of DRMSF to reveal the difference in mobility over all residues induced by a given R1 substitution. Sites of each substitution are labeled with vertical lines.

4. Conclusion

The experimental results for the eight R1-BSLA variants demonstrate a success of the computationally based rationale for choosing sites to incorporate a cysteine substitution for labeling with MTSL for EPR investigations. CD data confirm minimal perturbation to the protein secondary structure, and by considering hydrogen bonding interactions within the protein structure the R1-BSLA variants have no significant perturbation in enzyme function or thermal stability. Our original design strategy did not include consideration of hydrophobic clusters as we assumed that none of these residues would appear “surface exposed”. Interestingly, site V54, although not showing major perturbations to structure or function, did slightly impact local dynamics and is contained within an identified hydrophobic cluster in BSLA. Hence, for future investigations, the results suggest additional screening for amino acids involved in hydrophobic clustering be removed during selective filters for choosing sites for spin-labeling that would minimize perturbations to structure, dynamics, and function.

Conflicts of interest

There are no conflicts to declare.

Acknowledgements

We would like to thank Prof. Michael E. Harris (UF), for access to CD instrumentation, Prof. Dan Savin (UF) for helpful comments and suggestions, and Prof. Joel Karr (Colorado State University) for providing plasmids for BSLA and helpful suggestions regarding protein purification and stability.

Funding:

This study was supported by NSF (MCB-1715384 and CHE-2003366; GEF), NIH (S10 RR031603; GEF) NIH S10 OD021758-01A1 (UF Chemistry Mass Spectrometry Facility).

Author Contributions

A.M.J. and A.B. designed mutagenic primers performed PCR, confirmed sequencing, and optimized over-expression of all IA_3 constructs. A.M.J. performed all CD data collection and analysis, EPR data collection and analysis and wrote the initial manuscript draft with A.B. aiding in over-expressed and purified protein constructs utilized in CD studies. M.Z. and A.K. performed EasySpin fitting of EPR data. A.M.J. performed all molecular dynamic simulations and analyses under C.M.C. guidance and mentorship. K.M.D., A.M.J, C.M.C. and G.E.F edited the final manuscript.

AUTHOR INFORMATION

Corresponding Authors

Gail E. Fanucci − Department of Chemistry, University of Florida, P.O. Box 117200, Gainesville, Florida 32611; Email: fanucci@chem.ufl.edu

Coray Colina− Department of Chemistry, George and Josephine Butler Polymer Research Laboratory, and Department of Materials Science and Engineering University of Florida, P.O. Box 117200, Gainesville, Florida 32611; Email: colina@chem.ufl.edu

Authors

Afnan M. Jaufer − Department of Chemistry, and George and Josephine Butler Polymer Research Laboratory, University of Florida, P.O. Box 117200, Gainesville, Florida 32611; Email: m.mohamedjaufer@chem.ufl.edu

Adam Bouhadana− Department of Chemistry, University of Florida, P.O. Box 117200, Gainesville, Florida 32611; Email: abouhadana@ufl.edu

Amir Kharrazizadeh− Department of Chemistry, University of Florida, P.O. Box 117200, Gainesville, Florida 32611; Email: a.kharrazizadeh@ufl.edu

Mingwei Zhou − Department of Chemistry, University of Florida, P.O. Box 117200, Gainesville, Florida 32611; Email: mzhou1@chem.ufl.edu

Coray Colina− Department of Chemistry, George and Josephine Butler Polymer Research Laboratory, and Department of Materials Science and Engineering University of Florida, P.O. Box 117200, Gainesville, Florida 32611; Email: colina@chem.ufl.edu

References:

[1] E.J. Gilbert, Pseudomonas lipases: biochemical properties and molecular cloning, Enzyme Microb Technol 15 (1993) 634-645. 10.1016/0141-0229(93)90062-7.
[2] K.E. Jaeger, S. Ransac, B.W. Dijkstra, C. Colson, M. van Heuvel, O. Misset, Bacterial lipases, FEMS Microbiol Rev 15 (1994) 29-63. 10.1111/j.1574-6976.1994.tb00121.x.
[3] G. van Pouderoyen, T. Eggert, K.E. Jaeger, B.W. Dijkstra, The crystal structure of Bacillus subtilis lipase: a minimal alpha/beta hydrolase fold enzyme, J Mol Biol 309 (2001) 215-226. 10.1006/jmbi.2001.4659.
[4] A. Svendsen, Lipase protein engineering, Biochim Biophys Acta 1543 (2000) 223-238. 10.1016/s0167-4838(00)00239-9.
[5] H.L. Brockman, W.E. Momsen, T. T., Lipid-Lipid Complexes: Properties and Effects on Lipase Binding to Surfaces, J. Am. Oil Chem. Soc. 65 (1988) 891-896. doi.org/10.1007/BF02544505.
[6] S. Soni, Trends in lipase engineering for enhanced biocatalysis, Biotechnol Appl Biochem 69 (2022) 265-272. 10.1002/bab.2105.
[7] F.I. Khan, D. Lan, R. Durrani, W. Huan, Z. Zhao, Y. Wang, The Lid Domain in Lipases: Structural and Functional Determinant of Enzymatic Properties, Front Bioeng Biotechnol 5 (2017) 16. 10.3389/fbioe.2017.00016.
[8] C. Cambillau, S. Longhi, A. Nicolas, C. Martinez, Acyl glycerol hydrolases: inhibitors, interface and catalysis, Curr Opin Struct Biol 6 (1996) 449-455. 10.1016/s0959-440x(96)80108-4.
[9] D.W. Wong, Food Enzymes, Springer, Boston, MA, 1995.
[10] A.M. Brzozowski, H. Savage, C.S. Verma, J.P. Turkenburg, D.M. Lawson, A. Svendsen, S. Patkar, Structural origins of the interfacial activation in Thermomyces (Humicola) lanuginosa lipase, Biochemistry 39 (2000) 15071-15082. 10.1021/bi0013905.
[11] Y. Yang, M.E. Lowe, The open lid mediates pancreatic lipase function, J Lipid Res 41 (2000) 48-57.
[12] S. Brocca, F. Secundo, M. Ossola, L. Alberghina, G. Carrea, M. Lotti, Sequence of the lid affects activity and specificity of Candida rugosa lipase isoenzymes, Protein Sci 12 (2003) 2312-2319. 10.1110/ps.0304003.
[13] V. Belle, A. Fournel, M. Woudstra, S. Ranaldi, F. Prieri, V. Thome, J. Currault, R. Verger, B. Guigliarelli, F. Carriere, Probing the opening of the pancreatic lipase lid using site-directed spin labeling and EPR spectroscopy, Biochemistry 46 (2007) 2205-2214. 10.1021/bi0616089.
[14] S. Ranaldi, V. Belle, M. Woudstra, R. Bourgeas, B. Guigliarelli, P. Roche, H. Vezin, F. Carriere, A. Fournel, Amplitude of pancreatic lipase lid opening in solution and identification of spin label conformational subensembles by combining continuous wave and pulsed EPR spectroscopy and molecular dynamics, Biochemistry 49 (2010) 2140-2149. 10.1021/bi901918f.
[15] S. Behera, S. Balasubramanian, Lipase A from Bacillus subtilis: Substrate Binding, Conformational Dynamics, and Signatures of a Lid, J Chem Inf Model 63 (2023) 7545-7556. 10.1021/acs.jcim.3c01681.
[16] K. Kawasaki, H. Kondo, M. Suzuki, S. Ohgiya, S. Tsuda, Alternate conformations observed in catalytic serine of Bacillus subtilis lipase determined at 1.3 A resolution, Acta Crystallogr D Biol Crystallogr 58 (2002) 1168-1174. 10.1107/s090744490200714x.
[17] H.S. Yun, H.J. Park, J.C. Joo, Y.J. Yoo, Thermostabilization of Bacillus subtilis lipase A by minimizing the structural deformation caused by packing enhancement, J Ind Microbiol Biotechnol 40 (2013) 1223-1229. 10.1007/s10295-013-1330-2.
[18] S. Ahmad, M.Z. Kamal, R. Sankaranarayanan, N.M. Rao, Thermostable Bacillus subtilis lipases: in vitro evolution and structural insight, J Mol Biol 381 (2008) 324-340. 10.1016/j.jmb.2008.05.063.

[19] M.Z. Kamal, S. Ahmad, T.R. Molugu, A. Vijayalakshmi, M.V. Deshmukh, R. Sankaranarayanan, N.M. Rao, In vitro evolved non-aggregating and thermostable lipase: structural and thermodynamic investigation, J Mol Biol 413 (2011) 726-741. 10.1016/j.jmb.2011.09.002.
[20] H. Cui, M. Vedder, L. Zhang, K.E. Jaeger, U. Schwaneberg, M.D. Davari, Polar Substitutions on the Surface of a Lipase Substantially Improve Tolerance in Organic Solvents, ChemSusChem 15 (2022) e202102551. 10.1002/cssc.202102551.
[21] H. Cui, L. Eltoukhy, L. Zhang, U. Markel, K.E. Jaeger, M.D. Davari, U. Schwaneberg, Less Unfavorable Salt Bridges on the Enzyme Surface Result in More Organic Cosolvent Resistance, Angew Chem Int Ed Engl 60 (2021) 11448-11456. 10.1002/anie.202101642.
[22] E.M. Nordwald, G.S. Armstrong, J.L. Kaar, NMR-Guided Rational Engineering of an Ionic-Liquid-Tolerant Lipase, ACS Catal. 4 (2014) 4057-4064. 10.1021/cs500978x.
[23] S. Behera, S. Balasubramanian, Molecular simulations explain the exceptional thermal stability, solvent tolerance and solubility of protein-polymer surfactant bioconjugates in ionic liquids, Phys Chem Chem Phys 24 (2022) 21904-21915. 10.1039/d2cp02636h.
[24] Y. Zhou, N.C. Jones, J. Nedergaard Pedersen, B. Perez, S. Vronning Hoffmann, S. Vang Petersen, J. Skov Pedersen, A. Perriman, P. Kristensen, R. Gao, Z. Guo, Insight into the Structure and Activity of Surface-Engineered Lipase Biofluids, Chembiochem 20 (2019) 1266-1272. 10.1002/cbic.201800819.
[25] S. Behera, S. Balasubramanian, Insights into substrate behavior in a solvent-free protein liquid to rationalize its reduced catalytic rate, RSC Adv 12 (2022) 11896-11905. 10.1039/d2ra00666a.
[26] G.R. Chado, E.N. Holland, A.K. Tice, M.P. Stoykovich, J.L. Kaar, Modification of Lipase with Poly(4-acryloylmorpholine) Enhances Solubility and Transesterification Activity in Anhydrous Ionic Liquids, Biomacromolecules 19 (2018) 1324-1332. 10.1021/acs.biomac.8b00176.
[27] R. Kumar, S. Goomber, J. Kaur, Engineering lipases for temperature adaptation: Structure function correlation, Biochim Biophys Acta Proteins Proteom 1867 (2019) 140261. 10.1016/j.bbapap.2019.08.001.
[28] W. Augustyniak, A.A. Brzezinska, T. Pijning, H. Wienk, R. Boelens, B.W. Dijkstra, M.T. Reetz, Biophysical characterization of mutants of Bacillus subtilis lipase evolved for thermostability: factors contributing to increased activity retention, Protein Sci 21 (2012) 487-497. 10.1002/pro.2031.
[29] W. Augustyniak, H. Wienk, R. Boelens, M.T. Reetz, (1)H, (1)(3)C and (1)(5)N resonance assignments of wild-type Bacillus subtilis Lipase A and its mutant evolved towards thermostability, Biomol NMR Assign 7 (2013) 249-252. 10.1007/s12104-012-9420-z.
[30] Z. Xiao, X. Hou, X. Lyu, J.Y. Zhao, L. Xi, J. Li, J.R. Lu, Enzymatic synthesis of aroma acetoin fatty acid esters by immobilized Candida antarctica lipase B, Biotechnol Lett 37 (2015) 1671-1677. 10.1007/s10529-015-1834-0.
[31] S.A. Funke, A. Eipper, M.T. Reetz, N. Otte, W. Thiel, G. Van Pouderoyen, B.W. Dijkstra, K.E. Jaeger, T. Eggert, Directed Evolution of an Enantioselective Bacillus Subtilis Lipase, Biocatal. Biotransformation 21 (2003) 67-73.
[32] J. Lyu, Z. Li, M. J., R. Jiang, G. Tang, Y. Zhou, R. Gao, Covalent immobilization of Bacillus subtilis lipase A on Fe3O4 nanoparticles by aldehyde tag: An ideal immobilization with minimal chemical modification, Process Biochemistry 81 (2019) 63-69. https://doi.org/10.1016/j.procbio.2019.03.017.
[33] S. Das, S. Behera, S. Balasubramanian, Orientational Switch of the Lipase A Enzyme at the Oil-Water Interface: An Order of Magnitude Increase in Turnover Rate with a Single Surfactant Tag Explained, J Phys Chem Lett 11 (2020) 2977-2982. 10.1021/acs.jpclett.0c00470.
[34] R. Martinez, C. Bernal, R. Alvarez, C. Concha, F. Araya, R. Cabrera, G.V. Dhoke, M.D. Davari, Deletion and Randomization of Structurally Variable Regions in B. subtilis Lipase A (BSLA) Alter Its Stability and Hydrolytic Performance Against Long Chain Fatty Acid Esters, Int J Mol Sci 21 (2020). 10.3390/ijms21061990.

[35] L. Zhang, Y. Ding, The Relation Between Lipase Thermostability and Dynamics of Hydrogen Bond and Hydrogen Bond Network Based on Long Time Molecular Dynamics Simulation, Protein Pept Lett 24 (2017) 643-648. 10.2174/0929866524666170502151429.
[36] M. Klahn, G.S. Lim, P. Wu, How ion properties determine the stability of a lipase enzyme in ionic liquids: a molecular dynamics study, Phys Chem Chem Phys 13 (2011) 18647-18660. 10.1039/c1cp22056j.
[37] P.R. Burney, E.M. Nordwald, K. Hickman, J.L. Kaar, J. Pfaendtner, Molecular dynamics investigation of the ionic liquid/enzyme interface: application to engineering enzyme surface charge, Proteins 83 (2015) 670-680. 10.1002/prot.24757.
[38] P.R. Burney, J. Pfaendtner, Structural and dynamic features of Candida rugosa lipase 1 in water, octane, toluene, and ionic liquids BMIM-PF6 and BMIM-NO3, J Phys Chem B 117 (2013) 2662-2670. 10.1021/jp312299d.
[39] K. Huang, X. Fang, A review on recent advances in methods for site-directed spin labeling of long RNAs, Int J Biol Macromol 239 (2023) 124244. 10.1016/j.ijbiomac.2023.124244.
[40] L. Galazzo, M. Teucher, E. Bordignon, Orthogonal spin labeling and pulsed dipolar spectroscopy for protein studies, Methods Enzymol 666 (2022) 79-119. 10.1016/bs.mie.2022.02.004.
[41] I.D. Sahu, G.A. Lorigan, Site-Directed Spin Labeling EPR for Studying Membrane Proteins, Biomed Res Int 2018 (2018) 3248289. 10.1155/2018/3248289.
[42] P. Roser, M.J. Schmidt, M. Drescher, D. Summerer, Site-directed spin labeling of proteins for distance measurements in vitro and in cells, Org Biomol Chem 14 (2016) 5468-5476. 10.1039/c6ob00473c.
[43] D.S. Cafiso, Identifying and quantitating conformational exchange in membrane proteins using site-directed spin labeling, Acc Chem Res 47 (2014) 3102-3109. 10.1021/ar500228s.
[44] J.P. Klare, Site-directed spin labeling EPR spectroscopy in protein research, Biol Chem 394 (2013) 1281-1300. 10.1515/hsz-2013-0155.
[45] W.L. Hubbell, C.J. Lopez, C. Altenbach, Z. Yang, Technological advances in site-directed spin labeling of proteins, Curr Opin Struct Biol 23 (2013) 725-733. 10.1016/j.sbi.2013.06.008.
[46] H.S. McHaourab, P.R. Steed, K. Kazmier, Toward the fourth dimension of membrane protein structure: insight into dynamics from spin-labeling EPR spectroscopy, Structure 19 (2011) 1549-1561. 10.1016/j.str.2011.10.009.
[47] W.L. Hubbell, D.S. Cafiso, C. Altenbach, Identifying conformational changes with site-directed spin labeling, Nat Struct Biol 7 (2000) 735-739. 10.1038/78956.
[48] G.E. Fanucci, D.S. Cafiso, Recent advances and applications of site-directed spin labeling, Curr Opin Struct Biol 16 (2006) 644-653. 10.1016/j.sbi.2006.08.008.
[49] F. Torricella, A. Pierro, E. Mileo, V. Belle, A. Bonucci, Nitroxide spin labels and EPR spectroscopy: A powerful association for protein dynamics studies, Biochim Biophys Acta Proteins Proteom 1869 (2021) 140653. 10.1016/j.bbapap.2021.140653.
[50] G.K. Chow, A.G. Chavan, J.C. Heisler, Y.G. Chang, A. LiWang, R.D. Britt, Monitoring Protein-Protein Interactions in the Cyanobacterial Circadian Clock in Real Time via Electron Paramagnetic Resonance Spectroscopy, Biochemistry 59 (2020) 2387-2400. 10.1021/acs.biochem.0c00279.
[51] G.K. Chow, A. LiWang, R.D. Britt, Site directed spin labeling to elucidating the mechanism of the cyanobacterial circadian clock, Methods Enzymol 666 (2022) 59-78. 10.1016/bs.mie.2022.02.011.
[52] G.K. Chow, A.G. Chavan, J. Heisler, Y.G. Chang, N. Zhang, A. LiWang, R.D. Britt, A Night-Time Edge Site Intermediate in the Cyanobacterial Circadian Clock Identified by EPR Spectroscopy, J Am Chem Soc 144 (2022) 184-194. 10.1021/jacs.1c08103.
[53] D.A. Nyenhuis, T.D. Nilaweera, J.K. Niblo, N.Q. Nguyen, K.H. DuBay, D.S. Cafiso, Evidence for the Supramolecular Organization of a Bacterial Outer-Membrane Protein from In Vivo Pulse Electron Paramagnetic Resonance Spectroscopy, J Am Chem Soc 142 (2020) 10715-10722. 10.1021/jacs.0c01754.

[54] F. Kaiser, B. Endeward, A. Collauto, U. Scheffer, T.F. Prisner, M.W. Gobel, Spin-Labeled Riboswitch Synthesized from a Protected TPA Phosphoramidite Building Block, Chemistry 28 (2022) e202201822. 10.1002/chem.202201822.
[55] B. Endeward, Y. Hu, G. Bai, G. Liu, T.F. Prisner, X. Fang, Long-range distance determination in fully deuterated RNA with pulsed EPR spectroscopy, Biophys J 121 (2022) 37-43. 10.1016/j.bpj.2021.12.007.
[56] J.M. Franck, S. Han, Overhauser Dynamic Nuclear Polarization for the Study of Hydration Dynamics, Explained, Methods Enzymol 615 (2019) 131-175. 10.1016/bs.mie.2018.09.024.
[57] J.M. Franck, A. Pavlova, J.A. Scott, S. Han, Quantitative cw Overhauser effect dynamic nuclear polarization for the analysis of local water dynamics, Prog Nucl Magn Reson Spectrosc 74 (2013) 33-56. 10.1016/j.pnmrs.2013.06.001.
[58] J.L. Wort, K. Ackermann, D.G. Norman, B.E. Bode, A general model to optimise Cu(II) labelling efficiency of double-histidine motifs for pulse dipolar EPR applications, Phys Chem Chem Phys 23 (2021) 3810-3819. 10.1039/d0cp06196d.
[59] G. Jeschke, MMM: A toolbox for integrative structure modeling, Protein Sci 27 (2018) 76-85. 10.1002/pro.3269.
[60] M.H. Tessmer, S. Stoll, chiLife: An open-source Python package for in silico spin labeling and integrative protein modeling, PLoS Comput Biol 19 (2023) e1010834. 10.1371/journal.pcbi.1010834.
[61] X. Bogetti, S. Saxena, Integrating Electron Paramagnetic Resonance Spectroscopy and Computational Modeling to Measure Protein Structure and Dynamics, Chempluschem (2023) e202300506. 10.1002/cplu.202300506.
[62] E.F. Pettersen, T.D. Goddard, C.C. Huang, G.S. Couch, D.M. Greenblatt, E.C. Meng, T.E. Ferrin, UCSF Chimera--a visualization system for exploratory research and analysis, J Comput Chem 25 (2004) 1605-1612. 10.1002/jcc.20084.
[63] S. Jo, X. Cheng, S.M. Islam, L. Huang, H. Rui, A. Zhu, H.S. Lee, Y. Qi, W. Han, K. Vanommeslaeghe, A.D. MacKerell, Jr., B. Roux, W. Im, CHARMM-GUI PDB manipulator for advanced modeling and simulations of proteins containing nonstandard residues, Adv Protein Chem Struct Biol 96 (2014) 235-265. 10.1016/bs.apcsb.2014.06.002.
[64] S.M. Islam, R.A. Stein, H.S. McHaourab, B. Roux, Structural refinement from restrained-ensemble simulations based on EPR/DEER data: application to T4 lysozyme, J Phys Chem B 117 (2013) 4740-4754. 10.1021/jp311723a.
[65] B. Roux, S.M. Islam, Restrained-ensemble molecular dynamics simulations based on distance histograms from double electron-electron resonance spectroscopy, J Phys Chem B 117 (2013) 4733-4739. 10.1021/jp3110369.
[66] J. Huang, S. Rauscher, G. Nawrocki, T. Ran, M. Feig, B.L. de Groot, H. Grubmuller, A.D. MacKerell, Jr., CHARMM36m: an improved force field for folded and intrinsically disordered proteins, Nat Methods 14 (2017) 71-73. 10.1038/nmeth.4067.
[67] D.A.B. Case, K.; Ben-Shalom, I.; Brozell, S. R.; Cerutti, D.; Cheatham, T.; Cruzeiro, V. W. D.; Darden, T.; Duke, R. E.; Giambasu, G.; Gilson, M.; Gohlke, H.; Götz, A.; Harris, R.; Izadi, S.; Kasavajhala, K.; Kovalenko, A.; Krasny, R.; Kurtzman, T.; Lee, T.; LeGrand, S.; Li, P.; Lin, C.; Liu, J.; Luchko, T.; Luo, R.; Man, V.; Merz, K. M.; Miao, Y.; Monard, G.; Nguyen, H.; Onufriev, A.; Pan, F.; Pantano, S.; Qi, R.; Roe, D. R.; Roitberg, A.; Sagui, C.; Schott-Verdugo, S.; Shen, J.; Simmerling, C.; Smith, J.; Swails, J.; Walker, R.; Wang, J.; Wilson, L.; Wolf, R. M.; Wu, X.; Xiong, Y.; Xue, Y.; York, D.; Kollman, P. A., Amber 2020, University of California Press2020.
[68] A.C. Ramanathan, S. C.; Kabbani, N.; Olds, J. L.; Jha, S., Computational Approaches to Understand Molecular Mechanisms of SARS-CoV-2, Fronteirs Media, SA, 2022.
[69] W. Kabsch, C. Sander, Dictionary of protein secondary structure: pattern recognition of hydrogen-bonded and geometrical features, Biopolymers 22 (1983) 2577-2637. 10.1002/bip.360221211.

[70] T.E. Frederick, P.C. Goff, C.E. Mair, R.S. Farver, J.R. Long, G.E. Fanucci, Effects of the endosomal lipid bis(monoacylglycero)phosphate on the thermotropic properties of DPPC: A 2H NMR and spin label EPR study, Chem Phys Lipids 163 (2010) 703-711. 10.1016/j.chemphyslip.2010.06.002.
[71] S. Stoll, A. Schweiger, EasySpin, a comprehensive software package for spectral simulation and analysis in EPR, J Magn Reson 178 (2006) 42-55. 10.1016/j.jmr.2005.08.013.
[72] J.D. Carter, J.D. Mathias, E.F. Gomez, Y. Ran, F. Xu, L. Galiano, N.Q. Tran, P.W. D'Amore, C.S. Wright, D.K. Chakravorty, G.E. Fanucci, Characterizing Solution Surface Loop Conformational Flexibility of the GM2 Activator Protein, J Phys Chem B 118 (2014) 10607-10617. 10.1021/jp505938t.
[73] Z.C. Liang, Y. Lou, J.H. Freed, L. Columbus, W.L. Hubbell, A multifrequency electron spin resonance study of T4 lysozyme dynamics using the slowly relaxing local structure model, J Phys Chem B 108 (2004) 17649-17659. 10.1021/jp0484837.
[74] L. Columbus, W.L. Hubbell, Mapping backbone dynamics in solution with site-directed spin labeling: GCN4-58 bZip free and bound to DNA, Biochemistry 43 (2004) 7273-7287. 10.1021/bi0497906.
[75] L. Columbus, T. Kalai, J. Jeko, K. Hideg, W.L. Hubbell, Molecular motion of spin labeled side chains in alpha-helices: analysis by variation of side chain structure, Biochemistry 40 (2001) 3828-3846. 10.1021/bi002645h.
[76] J. Zhao, V.J. Frauenkron-Machedjou, A. Fulton, L. Zhu, M.D. Davari, K.E. Jaeger, U. Schwaneberg, M. Bocola, Unraveling the effects of amino acid substitutions enhancing lipase resistance to an ionic liquid: a molecular dynamics study, Phys Chem Chem Phys 20 (2018) 9600-9609. 10.1039/c7cp08470f.
[77] A.P. Todd, G.L. Millhauser, ESR spectra reflect local and global mobility in a short spin-labeled peptide throughout the alpha-helix----coil transition, Biochemistry 30 (1991) 5515-5523. 10.1021/bi00236a026.
[78] S.M. Miick, A.P. Todd, G.L. Millhauser, Position-dependent local motions in spin-labeled analogues of a short alpha-helical peptide determined by electron spin resonance, Biochemistry 30 (1991) 9498-9503. 10.1021/bi00103a016.
[79] J.T. Mindrebo, C.M. Nartey, Y. Seto, M.D. Burkart, J.P. Noel, Unveiling the functional diversity of the alpha/beta hydrolase superfamily in the plant kingdom, Curr Opin Struct Biol 41 (2016) 233-246. 10.1016/j.sbi.2016.08.005.
[80] M.Z. Kamal, T.A. Mohammad, G. Krishnamoorthy, N.M. Rao, Role of active site rigidity in activity: MD simulation and fluorescence study on a lipase mutant, PLoS One 7 (2012) e35188. 10.1371/journal.pone.0035188.
[81] A. Guidoni, F. Benkouka, J. De Caro, M. Rovery, Characterization of the serine reacting with diethyl p-nitrophenyl phosphate in porcine pancreatic lipase, Biochim Biophys Acta 660 (1981) 148-150. 10.1016/0005-2744(81)90120-0.
[82] I.F. Ma'ruf, M.P. Widhiastuty, Suharti, M.R. Moeis, Akhmaloka, Effect of mutation at oxyanion hole residu (H110F) on activity of Lk4 lipase, Biotechnol Rep (Amst) 29 (2021) e00590. 10.1016/j.btre.2021.e00590.
[83] F.S. Mickel, F. Weidenbach, B. Swarovsky, K.S. LaForge, G.A. Scheele, Structure of the canine pancreatic lipase gene, J Biol Chem 264 (1989) 12895-12901.
[84] A. Shrake, J.A. Rupley, Environment and exposure to solvent of protein atoms. Lysozyme and insulin, J Mol Biol 79 (1973) 351-371. 10.1016/0022-2836(73)90011-9.
[85] M.Z. Tien, A.G. Meyer, D.K. Sydykova, S.J. Spielman, C.O. Wilke, Maximum allowed solvent accessibilites of residues in proteins, PLoS One 8 (2013) e80635. 10.1371/journal.pone.0080635.
[86] D.R. Roe, T.E. Cheatham, 3rd, PTRAJ and CPPTRAJ: Software for Processing and Analysis of Molecular Dynamics Trajectory Data, J Chem Theory Comput 9 (2013) 3084-3095. 10.1021/ct400341p.
[87] A. Micsonai, E. Moussong, F. Wien, E. Boros, H. Vadaszi, N. Murvai, Y.H. Lee, T. Molnar, M. Refregiers, Y. Goto, A. Tantos, J. Kardos, BeStSel: webserver for secondary structure and fold prediction for protein CD spectroscopy, Nucleic Acids Res 50 (2022) W90-W98. 10.1093/nar/gkac345.
[88] B.M. Nestle, B. Hauer, Engineering of Flexible Loops in Enzymes., ACS Catal. 4 (2014) 3201-3211.

[89] H.S. McHaourab, T. Kalai, K. Hideg, W.L. Hubbell, Motion of spin-labeled side chains in T4 lysozyme: effect of side chain structure, Biochemistry 38 (1999) 2947-2955. 10.1021/bi9826310.
[90] H.S. McHaourab, M.A. Lietzow, K. Hideg, W.L. Hubbell, Motion of spin-labeled side chains in T4 lysozyme. Correlation with protein structure and dynamics, Biochemistry 35 (1996) 7692-7704. 10.1021/bi960482k.
[91] M.A. Lietzow, W.L. Hubbell, Motion of spin label side chains in cellular retinol-binding protein: correlation with structure and nearest-neighbor interactions in an antiparallel beta-sheet, Biochemistry 43 (2004) 3137-3151. 10.1021/bi0360962.
[92] T.F. Cunningham, M.S. McGoff, I. Sengupta, C.P. Jaroniec, W.S. Horne, S. Saxena, High-resolution structure of a protein spin-label in a solvent-exposed beta-sheet and comparison with DEER spectroscopy, Biochemistry 51 (2012) 6350-6359. 10.1021/bi300328w.
[93] T.F. Cunningham, S. Pornsuwan, W.S. Horne, S. Saxena, Rotameric preferences of a protein spin label at edge-strand beta-sheet sites, Protein Sci 25 (2016) 1049-1060. 10.1002/pro.2918.
[94] N. Ferruz, S. Schmidt, B. Hocker, ProteinTools: a toolkit to analyze protein structures, Nucleic Acids Res 49 (2021) W559-W566. 10.1093/nar/gkab375.